

Dielectric and magnetic properties of Fe- and Nb-doped $\text{CaCu}_3\text{Ti}_4\text{O}_{12}$ R. K. Grubbs, E. L. Venturini, P. G. Clem, J. J. Richardson, B. A. Tuttle, and G. A. Samara
Sandia National Laboratories, Albuquerque, New Mexico 87185, USA

(Received 20 January 2005; revised manuscript received 20 June 2005; published 23 September 2005)

Detailed studies of the properties of ceramic $\text{CaCu}_3\text{Ti}_4\text{O}_{12}$ (CCTO) have clarified the physics of this interesting material and revealed several features not reported before. The dielectric relaxational properties of CCTO are explained in terms of a capacitive-layer model, as for an inhomogeneous semiconductor, consisting of semiconducting grains and insulating grain boundaries as also concluded by others. The kinetics of the main [low-temperature (T)] relaxation reveal that two different thermally activated processes in CCTO grains control the dynamics. A likely candidate defect responsible for the two processes is the oxygen vacancy which is a double donor. A higher- T relaxation is determined by grain boundary conduction. Both Nb and Fe doping lowered both the apparent dielectric constant ϵ' and the dielectric loss, but increased Fe doping led to more dramatic effects. At 3 at. % Fe doping, the anomalous $\epsilon'(T)$ response was removed, making the CCTO an intrinsic, very-low-loss dielectric. The intrinsic $\epsilon'(\approx 75)$ and its T dependence are measured and shown to be largely determined by a low-lying soft TO phonon. At low T , cubic CCTO transforms into an antiferromagnetic phase at $T_N=25$ K. T_N is essentially independent of Nb doping (up to 4 at. %) and of hydrostatic pressure (up to ~ 7 kbar), but decreases significantly with Fe doping. Analysis of the high- T dependence of the magnetic susceptibility provided insight into the role of Fe as a dopant. Finally, an $\epsilon'(T)$ anomaly associated with the onset of antiferromagnetic order has been discovered, providing evidence for coupling between the polarization and sublattice magnetization. The possible origin of this coupling is discussed.

DOI: [10.1103/PhysRevB.72.104111](https://doi.org/10.1103/PhysRevB.72.104111)

PACS number(s): 77.22.Ch, 75.30.Kz, 81.40.Rs

I. INTRODUCTION

The “unusual” dielectric properties of $\text{CaCu}_3\text{Ti}_4\text{O}_{12}$ (CCTO) have been of much recent interest. The material has a distorted, complex cubic perovskite (ABO_3)-like structure with a large unit cell ($a \approx 7.4$ Å).^{1,2} The Cu ions form a square planar lattice on the A sites and are bonded to four oxygen atoms each, causing tilting of the TiO_6 octahedra.

Subramanian *et al.*¹ were the first to report a very large ($>10\,000$) and nearly temperature- (T -) independent apparent static dielectric constant ϵ' , for ceramic samples of CCTO at $T \geq 300$ K. Subsequent work on ceramic²⁻⁵ as well as single-crystal² samples confirmed this early work and revealed additional features. In particular, below ~ 200 K ϵ' exhibits relaxational behavior, ultimately dropping to a value of ~ 100 at the lowest T 's with the crystal structure remaining cubic and centrosymmetric down to at least 35 K.

While dipole relaxation models associated with the complex crystal structure of CCTO have been suggested to explain the dielectric response,^{2,3} it is now generally agreed that the observed behavior is not intrinsic. Rather, the dielectric response is due to barrier-layer capacitances associated with one or more of the following: grain boundaries, twin boundaries, dislocation networks, and Schottky barrier or interfacial polarization effects.^{1,4,6-10} A detailed first-principles study⁶ of the structure and lattice dielectric response of CCTO did not reveal any unusual features in the zone-center optical phonons and estimated the intrinsic lattice contribution to ϵ' to be ~ 40 . Cohen *et al.*⁹ explored various scenarios of conducting and insulating structures in an inhomogeneous solid that can lead to very large ϵ 's and that could agree with the observed response of CCTO. They considered cases where the bulk of the sample (or grain) is either con-

ducting or nearly so and the grain and domain boundaries are insulating, or vice versa. These studies show that large ϵ 's result either when the conducting regions approach a percolation threshold or when they percolate but are blocked at the sample surface or electrode interface. In CCTO oxygen vacancies and/or impurities can lead to conductivity in either the bulk (grains) or grain boundaries. Adams *et al.*⁷ suggested an explanation for the behavior of CCTO in terms of conducting grains and insulating grain boundaries. Strong support for this suggestion was provided by Chung *et al.*¹⁰ in the most definitive work thus far on undoped ceramic CCTO. Through a combination of microcontact I - V measurements, Kelvin probe force microscopy, and resistivity and thermoelectric power measurements on individual grains, as well as across grain boundaries, these authors have determined that (1) the grains are conducting and are n type, and (2) a large potential barrier exists at the grain boundaries reflecting their insulating character.

It has long been known¹¹ that CCTO exhibits an antiferromagnetic (AFM) transition at ~ 25 K. The transition region has been recently studied by neutron diffraction¹² and electron paramagnetic resonance (EPR),¹³ and the antiferromagnetism has been explained in terms of a double primitive cell in which each Cu-Cu nearest-neighbor pair has antiparallel spins. The behavior of the dielectric response near this transition apparently has not yet been studied.

The purpose of the present work is to investigate the effects of doping (Nb and Fe) and hydrostatic pressure on the dielectric properties and AFM transition of CCTO in order to shed additional light on the interesting properties of this complex oxide. Also, we sought evidence (which we found) for a possible coupling between the magnetization and polarization below the AFM transition or Neel temperature T_N . Consequently, a considerable part of our effort was devoted

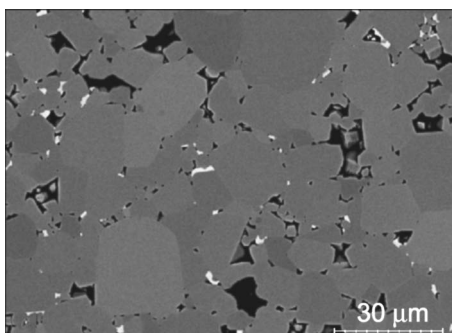


FIG. 1. A typical microstructure of our ceramic CCTO samples as determined by SEM.

to the low-temperature properties where the response of CCTO can be expected to become essentially intrinsic. Doping with iron (Fe) allowed us to reach the intrinsic regime where we found the behavior of $\epsilon'(T)$ to be different from that suggested by earlier work. Iron doping is also found to produce remarkably large changes in the overall dielectric response. In what follows we shall first give a brief description of the experimental details in Sec. II followed by a presentation and discussion of the results in Sec. III.

II. EXPERIMENTAL DETAILS

A. Samples

Ceramic $\text{CaCu}_3\text{Ti}_4\text{O}_{12}$ (pure, as well as Fe or Nb doped) pellets were prepared using a solid-state reaction and sintering process. Precursor powders of CaCO_3 ($\geq 99.95\%$ Aldrich), TiO_2 ($\geq 99.8\%$ Aldrich), and CuO ($\geq 99.99\%$ Aldrich) were directly combined in the necessary stoichiometric ratios while doped samples employed Fe_2O_3 ($\geq 99.3\%$ Baker Chemical) as a powder or Nb *n*-butoxide ($\geq 99\%$ Inorgtech) in ethanol, as dopant precursors. Thorough mixing was achieved by milling the powders in ethanol or acetone with zirconia media for no less than 12 h in a rolling mill. The dried mixed powders were calcined at 1173 K (900 °C) for 1 h before being milled a second time. The dried powders were uniaxially cold pressed into $\frac{1}{2}$ in. pellets under a load of 2000 lb (~ 10 ksi pressure). The resulting pellets were then sintered in air on top of Pt setters (to avoid reaction with the ceramic alumina furnace boats) using the schedule 10 K/min to 1273 K (1000 °C), 6 h hold, 10 K/min to 1373 K (1100 °C), 6 hour hold, and then furnace cooled to room temperature. After sintering, the pellets were confirmed to be polycrystalline, predominantly single-phase, $\text{CaCu}_3\text{Ti}_4\text{O}_{12}$ by θ -2 θ x-ray diffraction (XRD). Figure 1 shows a typical microstructure of CCTO revealing a broad distribution of grain sizes. The picture in Fig. 1 shows an enhanced contrast scanning electron microscope (SEM) image with the light colored areas identified as Cu rich. Interestingly, no second phases were observed on logarithmic-scale XRD scans of CCTO.

To control the defect chemistry of perovskite ABO_3 oxides such as BaTiO_3 , SrTiO_3 and $\text{Pb}(\text{Zr},\text{Ti})\text{O}_3$ (PZT), a variety of dopants have been developed to occupy the A- and B-site cation positions.^{14–16} Tailoring materials by way of

defect chemistry, including cation and oxygen vacancy concentration, with aliovalent cation dopants enables control of their semiconducting behavior, including free carrier type, carrier concentration, and hence, material resistivity and real and imaginary permittivity. In this work, $\text{CaCu}_3\text{Ti}_4\text{O}_{12}$ was modeled as a $4(\text{ABO}_3)$ perovskite where ideal cation charges would be +2 for the A-site and +4 for the B-site cations. Similar to the presence of lead vacancies inducing oxygen vacancies and *p*-type behavior in PZT, copper volatility and reduction of Cu from +2 to +1 was anticipated to produce oxygen-vacancy-related conductivity in CCTO.¹⁶ A number of dopants were selected on the basis of literature reports of *n*- and *p*-type perovskite dopants and prediction of dopant types by consideration of ionic radius and charge state.¹⁷ Niobium is a commonly used *n*-type dopant, as Nb^{5+} (ionic radius $r=0.64$ Å) it occupies a Ti^{4+} ($r=0.68$ Å) site, while Fe^{3+} ($r=0.55$ Å) was predicted to be a *p*-type dopant on the Ti^{4+} site. Samples were doped with 0–4 % of Nb or Fe substituting for Ti, as such doping levels are typically within the solid solution solubility limit for perovskites and were found to display single-phase CCTO x-ray diffraction patterns.

For dielectric measurements, sections of the pellets were cut using a diamond saw (typically cut into 4×4 mm² squares that were 0.50 mm thick), and polished. Consistent results came from samples cut from the center of the pellet. These will be denoted CCTO sample A. Similar, but lower-magnitude, dielectric responses were observed from samples cut from the end of the pellet. The dielectric response from an edge-cut sample is included in this study and is labeled CCTO sample B. Metal electrodes were rf magnetron sputter deposited on the samples. Initially, a thin film of Cr, approximately 650 Å thick, was used as an adhesion metal before 1000 Å of Au was deposited. The electroded samples were rigidly mounted between two copper paddles and a small quantity of silver paint was used to form an intimate contact between the Cu paddles and the metalized sample surface. The measurements were made with the sample placed in a He pressure cell that was in turn housed in a temperature Dewar.

B. Measurements

The real (ϵ') and imaginary (ϵ'' , or the loss factor $\tan \delta = \epsilon''/\epsilon'$) components of the dielectric function were measured with an Agilent 4284A LCR meter as functions of temperature (5–400 K), hydrostatic pressure (0–7 kbar), and frequency (100 Hz–1 MHz). No thermal hysteresis was observed for any of the samples used in this study. For the pressure experiments helium was the pressure-transmitting medium. A commercial superconducting quantum interference design magnetometer was used for the magnetic measurements at 1 bar. The pressure dependence of T_N was assessed from the pressure dependence of the anomaly of $\epsilon'(T)$ at T_N . Analysis of $\epsilon'(T)$ at low temperatures (i.e., in the intrinsic regime) required knowledge of the thermal expansion and volume compressibility of CCTO. The thermal expansion below 300 K was reported by Ramirez *et al.*³ and the volume compressibility was assumed to be comparable to that of other complex perovskites.

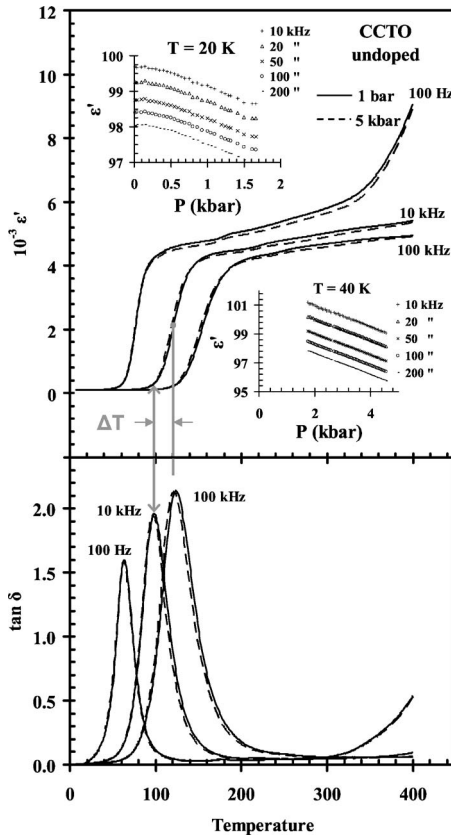


FIG. 2. Typical dielectric response of an undoped CCTO sample (sample B) at 1 bar and under the influence of hydrostatic pressure. The insets show the pressure dependence of ε' at two low temperatures and the finite ΔT suggests a nondipolar relaxation.

III. RESULTS AND DISCUSSION

A. Dielectric properties

In the course of this work we carried out detailed studies of the properties of undoped ceramic CCTO samples. The shapes and magnitudes of the $\varepsilon'(T)$ and $\tan \delta(T)$ curves as well as the frequency dispersions of the samples are very similar to the now familiar response of CCTO.^{2-5,8} A typical $\varepsilon'(T)$ response for CCTO is shown in Fig. 2. However, our results revealed additional features in the relaxational dynamics which are presented in Sec. III B.

We also investigated the influence of hydrostatic pressure on the dielectric response. Figure 2 shows that a pressure of 5 kbar (very modest compression) has very little influence on $\varepsilon'(T)$, generally causing small decreases in the magnitude of ε' at fixed T . The decrease in ε' due to pressure is seen most clearly in the low- T regime depicted in the two insets. We note that the $\varepsilon'(P)$ slopes at the two temperatures (20 and 40 K) are essentially independent of frequency. Over the narrow pressure ranges covered in the insets, one would expect the $\varepsilon'(P)$ response to be linear. Thus, the nonlinear $\varepsilon'(P)$ at the very lowest pressures at 20 K may reflect the influence of the AFM phase (Sec. III D). The weak pressure dependence of ε' observed in CCTO is consistent with the barrier-capacitance model for the dielectric response as these modest pressures are not expected to significantly change the prop-

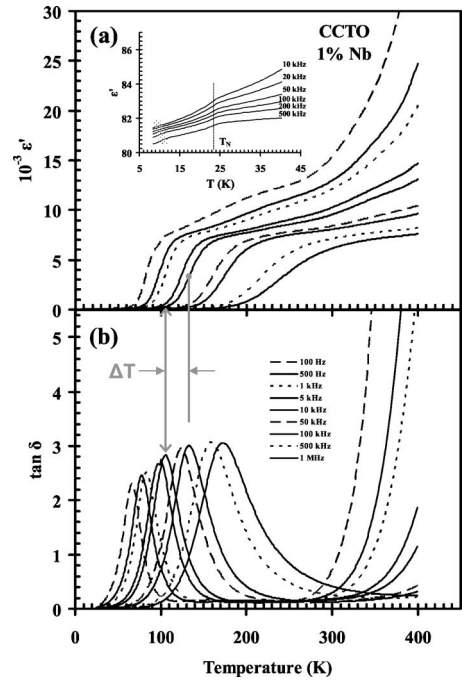


FIG. 3. Temperature dependences of ε' and $\tan \delta$ for a 1 at. % Nb-doped CCTO sample at different frequencies at 1 bar. The inset in (a) shows details of the $\varepsilon'(T)$ response to low temperatures and the finite ΔT suggests a nondipolar relaxation.

erties of the grains or grain boundaries and their thicknesses.

As noted earlier, our doping studies with Fe and Nb were aimed at modifying the electronic transport in CCTO to control the dielectric loss. Expecting that Fe^{3+} and Nb^{5+} would substitute primarily at the Ti^{4+} site, then Fe^{3+} would make the material p type and Nb^{5+} would make it n type. Figure 3 shows the dielectric response of a 1 at. % Nb doped sample. These results are qualitatively similar to those for the undoped CCTO samples. A 4 at. % Nb doped sample also showed similar results, but $\varepsilon'(T)$ in the plateau region was lower than that for the 1% Nb sample.

A decrease of ε' in the plateau regime with Nb doping is consistent with recent observations by Aygun *et al.*⁵ that showed a decrease of ε' with increased doping for samples doped with Nb and annealed in an oxygen atmosphere. We believe, as is also predicted from the grain and grain boundary capacitive-layer model, that the primary reason for this effect is an increase in grain boundary (oxide) layer thickness resulting in lower grain boundary capacitance, the change in grain resistivity with doping being relatively modest and inconsequential.

The low- T dielectric properties of the 1 and 4 at. % Nb-doped samples are very similar to those of the undoped samples. The low- T results for the 1% Nb sample are shown in the inset in Fig. 3(a). It is seen that the response at the lowest temperatures is still very dispersive, but additional features are revealed. The break in the $\varepsilon'(T)$ slope at 24 K, which also shows up as a slight bump in $\tan \delta(T)$, is a feature that is associated with the AFM transition at the Néel temperature, T_N . We shall come back to this feature below. Another feature in the low- T data is a relaxational process at ~ 10 K. It is somewhat similar in shape to the anomaly at T_N ,

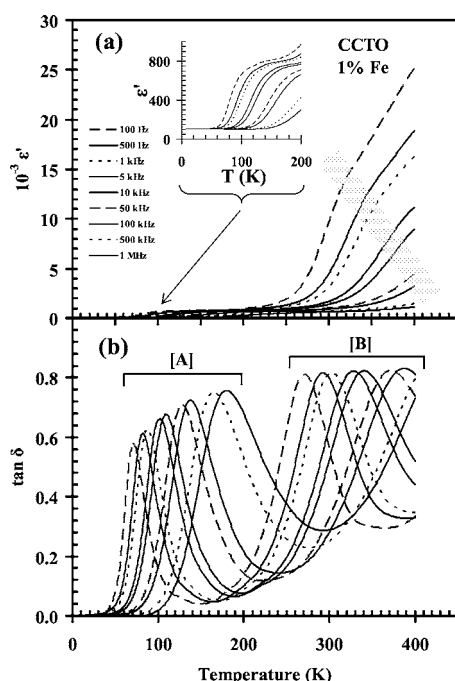


FIG. 4. Temperature dependences of ϵ' and $\tan \delta$ for a 1 at. % Fe-doped CCTO sample at different frequencies at 1 bar. The inset expands the $\epsilon'(T)$ response below 200 K.

but unlike the latter which is frequency independent, it exhibits strong frequency dispersion. It is likely due to a dipolar impurity or defect of unknown origin.

The response of a 1 at. % Fe-doped CCTO sample is shown in Fig. 4. In Fig. 4(a) we note the very marked reduction in the values of ϵ' in the plateau region (inset)—from many thousands for undoped and Nb-doped CCTO to several hundreds for the 1 at. % Fe sample. Associated with the reduced ϵ' is a large reduction in the peak value of $\tan \delta$ shown in Fig 4(b). This value goes from 2 to 3 for the samples in Figs. 2 and 3 to ~ 0.7 for 1 at. % Fe. Despite these differences, the low- T relaxation labeled [A] in Fig. 4(b) occurs in the same temperature range of 50–250 K as for the other CCTO samples.

Fe doping causes additional features not observed in the other samples over the temperature range of the present measurements (but expected at higher T 's, as will be discussed later). Figure 4 reveals a relaxational feature at higher T in both $\epsilon'(T)$ and in $\tan \delta(T)$, represented by the group of peaks labeled [B]. The dynamics of this feature will be discussed in Sec. III C below.

Fe doping also strongly influences the low-temperature response. The low- T results for 1 at. % Fe are shown in Fig. 5. First, note the increase of ϵ' with decreasing T above T_N . Second, note that the dielectric loss shown in the inset is much lower and the frequency dispersion much less than for the other samples. Both properties suggest that this sample is closer to exhibiting intrinsic behavior at low temperatures (explained in Sec. III B below). Also worth noting is that the relaxational process near 10 K is still present in this Fe-doped sample, confirming that it is associated with a dipolar entity characteristic of (ceramic) CCTO.

Increasing the Fe dopant concentration from 1 to 3 at. % produces further remarkable changes in the dielectric re-

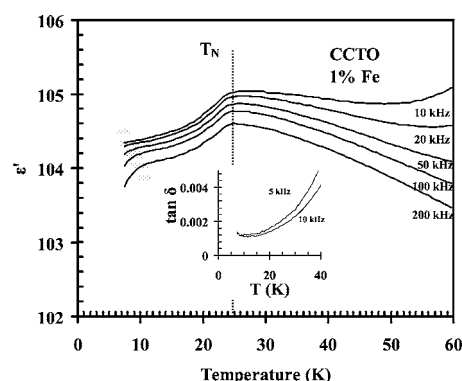


FIG. 5. A detailed view of the $\epsilon'(T)$ response of the 1 at. % Fe-doped sample at low temperatures. The inset shows the temperature dependence of the dielectric loss.

sponse of CCTO. Figures 6–8 show these results. Figures 6 and 7 show dielectric response of the 3 at. % Fe-doped CCTO sample. There is a dramatic decrease in the magnitude of ϵ' compared to the 1 at. % Fe sample (cf. Fig. 4). Both the values of ϵ' in the “plateau” region and $(\tan \delta)_{\max}$ are an order of magnitude lower than those of the 1 at. % Fe sample (and about two orders of magnitude lower than the undoped samples). There is also a noticeable shift in the plateau region to higher temperatures. The high- T relaxational peaks observed in Fig. 6(b) are similar to the [B] relaxations seen in the 1 at. % Fe sample in Fig. 4(b).

The mid-temperature region of 50–250 K for the 3 at. % Fe CCTO sample is shown in Fig. 7. It is seen that both the $\epsilon'(T)$ and $\tan \delta(T)$ relaxations (labeled [A*] for this sample)

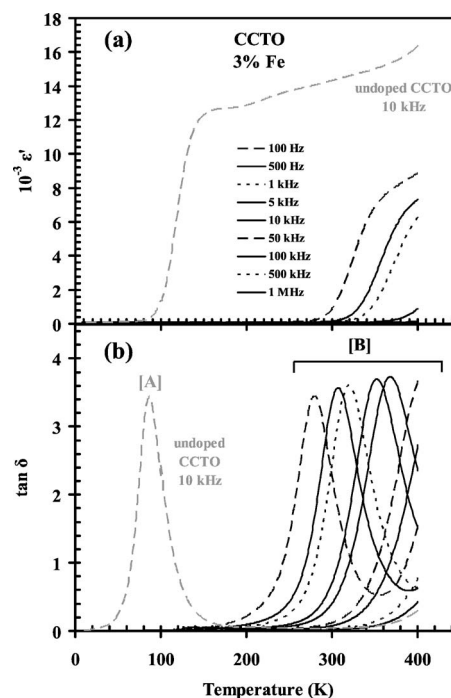


FIG. 6. Temperature dependences of ϵ' and $\tan \delta$ for a 3 at. % Fe-doped sample showing the suppression of the $\epsilon'(T)$ plateau below ~ 250 K. The dielectric response of undoped CCTO at 10 kHz is plotted for comparison.

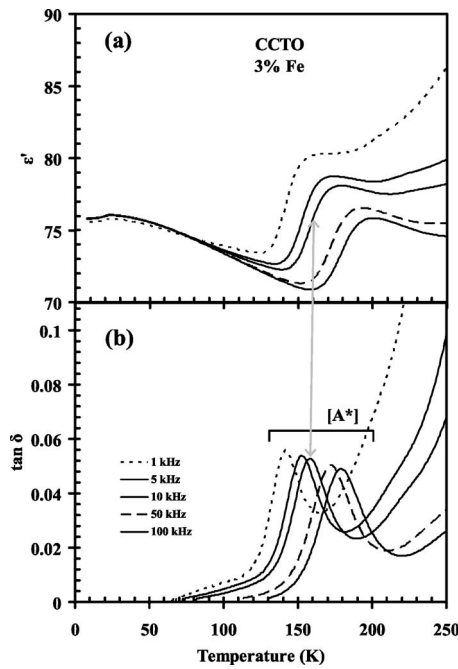


FIG. 7. Dipolar relaxational response of the 3 at. % Fe-doped sample.

have qualitatively different character from those observed in the 1 at. % Fe sample in Fig. 4(b) (relaxation labeled [A]) as well as in the other CCTO samples studied. Note in particular that the inflection point in the $\epsilon'(T)$ trace and the peak in the $\tan \delta(T)$ occur at the same temperature as indicated by the double arrow on the 10 kHz curve. This suggests that this particular relaxation is due to a dipolar entity in the sample and not due to extrinsic barrier-layer capacitances created between grains and grain boundaries, as was the case for all the other samples studied. As will be discussed in Sec. III B below, the $[A^*]$ relaxation in Fig. 7(b) exhibits different kinetics from those exhibited by the $[A]$ relaxations in other samples.

Figure 8 shows the results for the 3 at. % Fe CCTO sample below ~ 100 K. Here, the ϵ' values are 25–30 % lower than for the 1 at. % Fe sample and the frequency dispersion and dielectric loss are becoming vanishingly small. Thus, the dissipative mechanisms are essentially frozen and the dielectric response should be close to the intrinsic re-

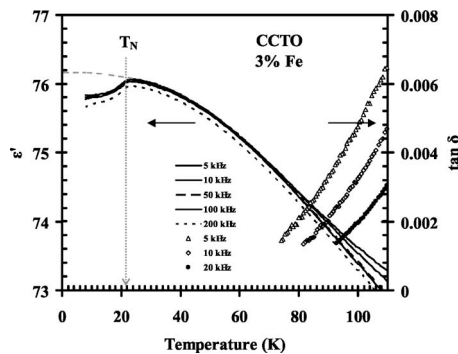


FIG. 8. The intrinsic dielectric response of the 3 at. % Fe-doped sample showing soft-mode behavior and the $\epsilon'(T)$ anomaly at T_N .

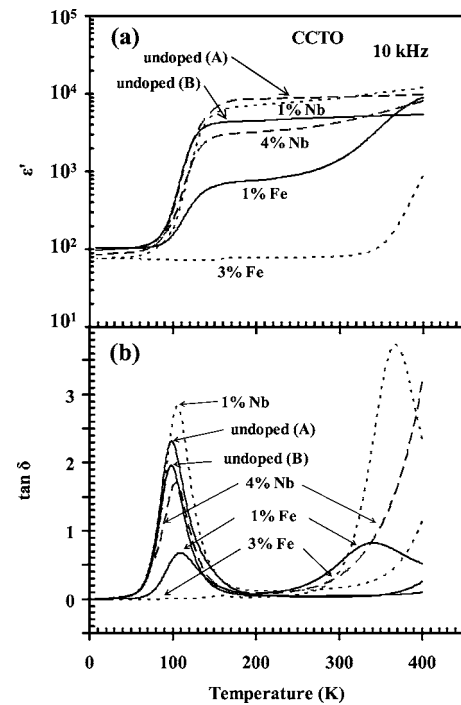


FIG. 9. Summary figure showing the influence of Nb and Fe doping on the dielectric response of CCTO.

sponse of the sample. In this regard the *increase* in ϵ' with *decreasing* T is characteristic of soft to mode behavior. The light dashed line below T_N in Fig. 8 would be the dielectric response of the sample in the absence of AFM ordering. This extrapolation clearly shows that $d\epsilon'/dT$ would go to 0 as $T \rightarrow 0$ K, as required by the third law of thermodynamics. We note that the $\epsilon'(T)$ anomaly associated with AFM transition is now seen at $T_N = 21$ K.

Clearly, there are significant doping effects associated with the 3 at. % Fe in CCTO that reflect important changes in the conductivity of either the grains and/or grain boundaries, with increasing Fe concentration. We shall discuss these effects in Sec. III B.

Figure 9 provides a summary of the $\epsilon'(T)$ and $\tan \delta(T)$ results for all of the samples used in this study at one frequency (10 kHz). Here, one can observe the remarkable influence that the addition of Fe has on the dielectric response of CCTO. All these results (except the 3 at. % Fe-doped sample) can be qualitatively understood in terms of the conducting grain and insulating grain boundary model cited in the Introduction. The physics of this model has been known for a long time. In the case of the 3 at. % Fe-doped sample, the relaxation around 150 K in Fig. 7 is, as already noted, of dipolar origin, and it is seen only when $\epsilon'(T)$ and $\tan \delta(T)$ approach intrinsic values. It may be due to an Fe-induced dipolar defect, or it may be present in all CCTO samples, but it is generally not observed in the dielectric data because it is hidden under the huge $\epsilon'(T)$ and $\tan \delta(T)$ responses associated with the barrier layers (compare, e.g., Figs. 3 and 7).

In the course of this work we noted a correlation between the magnitude of ϵ' in the plateau region and the peak value of $\tan \delta$ for the low-temperature $[A]$ relaxation. It was apparent that a larger ϵ' in the plateau region correlated with a

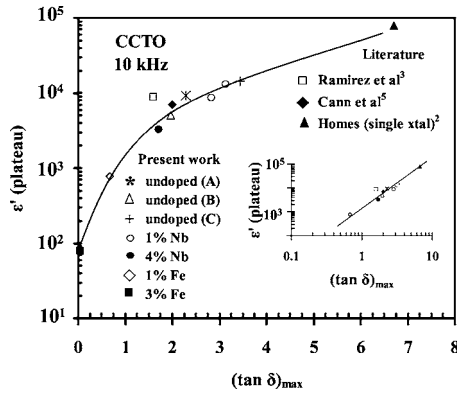


FIG. 10. Correlation between the value of ε' in the $\varepsilon'(T)$ plateau region and the maximum value of $\tan \delta$. The inset shows this correlation on a log-log plot.

larger value of the $\tan \delta$ peak maximum. This correlation is shown for our samples at a frequency of 10 kHz in Fig. 10. We have also included on this plot some of the data in the literature on ceramic samples that published both ε' and $(\tan \delta)_{\max}$ at 10 kHz. It is seen that all the data accurately follow the same trend which is qualitatively predicted by the barrier-layer-capacitance model.¹⁸

The discussion thus far has dealt with ceramic samples. But what about single-crystal CCTO? Homes *et al.*² studied the dielectric response of single-crystal CCTO and found results qualitatively similar to those for ceramic samples, but both the plateau values of ε' and the peak $\tan \delta$ values were much larger in magnitude. We have plotted their results at 10 kHz as a solid triangle in Fig. 10. Clearly, their datum point follows the trend observed for ceramic samples. The single crystal, of course, does not have the grains and grain boundaries alluded to in the barrier-layer-capacitance model. However, the single crystals do possess two interfaces and a bulk crystal interior which could display different resistivity characteristics and thus similar RC barrier properties to ceramic samples. It is also possible that a Schottky barrier or interfacial polarization effect is at work. The dielectric response of such a barrier on a semiconducting crystal is akin to that for the grain and grain boundary model.⁸ It has also been observed that grains of CCTO have a high concentration of dislocation lines and twin boundaries that are likely present in the single crystal.⁵ Such features can in principle lead to barrier layers that can contribute to the observed dielectric response of the crystal. Clearly more work on single-crystal CCTO is needed to better define the observed physics.

B. The relaxational dynamics of CCTO

Except for the 3 at. % Fe-doped sample, the low- T dielectric relaxations labeled [A] of the CCTO samples we examined are not dipolar in nature, but arise from the resistance-capacitance (or RC) properties of the barrier layers.¹⁸ Thus, they are not Debye relaxors, but exhibit Debye-like relaxations with Arrhenius kinetics [$1/\tau = \omega = \omega_0 \exp(-E/kT)$], as observed by others.^{2,3} A very significant feature of the RC barrier-layer model is that the relaxation time deduced from the $\varepsilon'(T, \omega)$ data, $\tau_{\varepsilon'}$, is longer than that deduced from the

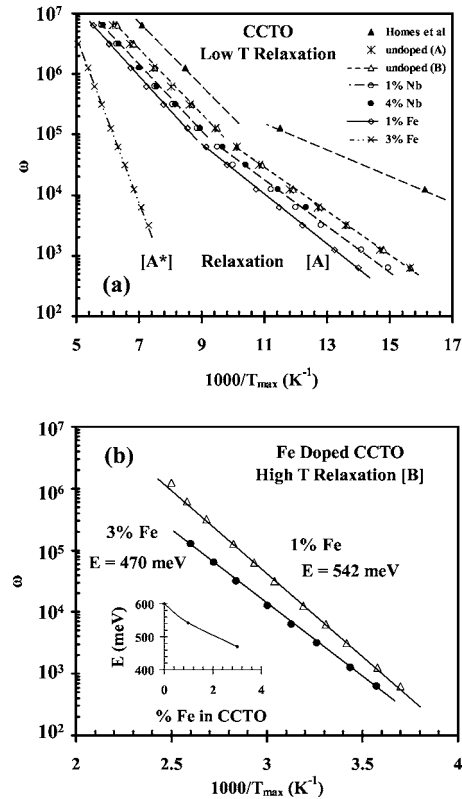


FIG. 11. Arrhenius plots for the observed relaxations. (a) Low-temperature relaxation [A] showing the two different thermally activated regions and the [A*] relaxation for the 3 at. % Fe-doped sample. (b) shows the high-temperature relaxation for the 1 and 3 at. % Fe-doped samples. The inset in (b) shows the variation of the activation energy with Fe doping.

$\tan \delta(T, \omega)$ data, τ_{δ} . This is reflected in Figs. 2 and 3 by ΔT which is the difference in T between the inflection point in the ε' relaxation, which determines $\tau_{\varepsilon'}$, and the peak T in the $\tan \delta$ relaxation, which determines τ_{δ} . For a dipolar relaxation process, $\tau_{\varepsilon'} \equiv \tau_{\delta}$. The relatively large values of ΔT in Figs. 2 and 3 are clear indications of the nondipolar nature of the relaxation in CCTO.

Figure 11(a) and Table I summarize our results for relaxation [A]. In the figure, T_{\max} is the temperature of the $\tan \delta$ peak at a given ω . It is seen that the response of all the samples (except the 3 at. % Fe sample) exhibit two Arrhenius segments, each with a distinct activation energy E . Thus, there are two separate activated conduction processes contributing to the relaxation labeled [A]. The data from all the samples are fairly tightly bunched together yielding essentially the same activation parameters E and $\omega_0 (=1/\tau_0)$, for all the samples. We have also plotted in Fig. 11(a) the sparse single-crystal data of Homes *et al.*² Although these authors drew a straight line through their data points, deducing $E = 54$ meV and $\omega_0 = 8.4 \times 10^{-9}$ Hz, the results are clearly either non-Arrhenius or indicate two Arrhenius segments as suggested by the dashed lines through the solid triangles. The activation energy of the high- T segment is the same (~ 110 meV) as for our ceramic samples, but for the lower- T segment the suggested E is significantly lower than the activation energy for the ceramic CCTO samples.

TABLE I. Arrhenius kinetic parameters for various ceramic CCTO samples for two relaxation processes. See text for details.

Sample	E (meV)	$\omega_0(\text{s}^{-1})$	E (meV)	$\omega_0(\text{s}^{-1})$
Low- <i>T</i> Arrhenius segment (a) Relaxation [A]			High- <i>T</i> Arrhenius segment	
Undoped (A)	71	1.8×10^8	104	1.0×10^{10}
Undoped (B)	71	2.6×10^8	106	1.3×10^{10}
1% Nb doped	71	1.3×10^8	110	9.7×10^9
4% Nb doped	74	2.5×10^8	109	9.9×10^9
1% Fe doped	81	3.2×10^8	113	8.8×10^9
3% Fe doped			268	2.1×10^{13}
(b) Relaxation [B]				
Undoped	600 ^a			
1% Fe doped	542	6.8×10^{12}		
3% Fe doped	470	1.8×10^{11}		

^aFrom Sinclair *et al.* (Ref. 4) determined from complex impedance data.

According to the grain and grain boundary model, these activation energies reflect the activation of conduction mechanisms in the grains.¹⁸ In terms of magnitudes, the E 's for both segments are consistent with values for other semiconducting titanate perovskites.⁴ Sinclair *et al.*⁴ obtained an activation energy for the bulk, or grains, of $E=80$ meV from complex impedance measurements. Their data covered a narrower T range than our own, and consequently they observed only one Arrhenius segment. Their 80 meV value for the grains fits in between our values for the two Arrhenius segments.

Given that the E for the higher- T segment for the single crystal agrees with the comparable E 's for the ceramics, we suggest that it represents the activation of the primary grain conduction mechanism in CCTO. As for the activation energy of the lower- T Arrhenius segment, we note from Fig. 11(a) that the suggested E for the single crystal may be considerably lower than the E 's for the ceramic samples, but there are not sufficient data points to be certain. This observation, coupled with the fact that E in this regime for the ceramics is essentially independent of doping, suggests that we are dealing with an electronic trap of an impurity or defect commonly present in CCTO.

A very likely candidate defect that may be responsible for the two observed activated segments in Fig. 11(a) is the oxygen vacancy V_O . This defect is undoubtedly introduced at a sufficiently high concentration during high- T crystal growth and ceramic processing. V_O is known to be responsible for the semiconducting behavior of many oxide perovskites.^{4,19,20} It acts as a double donor introducing two levels into the host's band gap lying about ~ 50 – 100 and 100 – 200 meV, respectively, below the conduction-band edge, depending on the material. These energies are sufficiently close to our measured activation energies of $E \sim 73$ and 108 meV so as to make the role of V_O in CCTO quite credible.

The results in Fig. 11(a) show that Nb doping and Fe doping at the 1 at. % level have no influence on the low- T conduction process in CCTO. However, the results for the 3 at. % Fe-doped sample are very different. The response [A*]

is that of a true dipolar relaxor with a single Debye relaxation time and kinetic parameters of $E=268$ meV and $\omega_0 = 2.12 \times 10^{13}$ Hz. The nature of the dipolar entity responsible for this relaxation is not known. It could of course be due to an off-center substitutional Fe ion or an Fe-induced defect. As discussed in Sec. III A, the only reason we are able to resolve this relaxation for 3 at. % Fe is because, at this doping level, the Fe reduces the dielectric loss (conductivity) and ϵ' to such a large extent that the sample exhibits essentially its intrinsic dielectric response. It may well be that this dipolar relaxation is present in all samples (i.e., it is not Fe related), but it is not resolved because it is swamped by the huge ϵ 's and $\tan \delta$ peaks of the other CCTO samples.

Our initial supposition and motivation for adding Fe was that Fe would substitute at the Ti^{4+} (B site) producing holes. The results on the 3% Fe sample and our magnetic data, to be presented in Sec. III D below, indicate that much of the Fe^{3+} substitutes at the Ti^{4+} site. The holes introduced by this Fe doping could then compensate for the conduction electrons contributed by the oxygen vacancies, leading to essentially intrinsic behavior of the CCTO grains. Our results support this view.

Another important feature in our results on the 1 and 3 at. % Fe-doped samples is the high- T relaxation labeled [B] in Figs. 4 and 6. This Debye-like relaxation exhibits Arrhenius kinetics as shown in Fig. 11(b) with the parameters listed in Table I. The rapid increase in $\tan \delta$ with increasing T above 350 K in Fig. 3 (also observed for undoped CCTO) suggests that this relaxation may be obtained for the undoped and Nb-doped samples at $T > 400$ K (beyond the range of the apparatus used).

In terms of the barrier-layer model, this [B] relaxation is attributed to the grain-boundary region and thus the activation energies in Table I and in Fig. 11(b) reflect E for the conduction process in this region. This is the region that controls dc transport. The activation energies of $E=542$ and 470 meV for the 1 and 3 at. % Fe samples, respectively, are characteristic of activation energies for dc electronic transport in many oxides. Sinclair *et al.*⁴ deduced a grain boundary activation energy of 600 meV for undoped CCTO from

complex impedance data. This value fits with our results on the Fe-doped samples which reveal a decrease in E with increasing Fe content—a monotonic dependence as shown in the inset in Fig. 11(b).

C. The intrinsic static dielectric constant of CCTO

Our low- T results in Figs. 2–4 as well as data in the literature³ on bulk ceramic samples gave initial indications that the intrinsic value of ϵ' of CCTO ≈ 100 . Tselev *et al.*²¹ reached a similar conclusion from results on thin film CCTO grown epitaxially on LaAlO_3 , although their data extended only down to ~ 80 K. However, as we have already seen in Figs. 2–4 a relatively strong frequency dispersion is observed in all of these samples down to the lowest temperatures, indicating extrinsic behavior. The clear exception is the 3 at. % Fe-doped sample shown in Fig. 8. Ignoring a possible influence of the Fe dopant on the magnitude of ϵ' , these latter results, which exhibit no frequency dispersion and show an ϵ' that *increases* with *decreasing* T , indicate that they represent the *intrinsic* behavior of ϵ' with a value of ~ 75 at the lowest T 's. Let us explain.

A value of ϵ' of ~ 75 is large for a normal ionic crystal. What is the origin of such a large value? In the absence of dipolar centers, ϵ' of an ionic crystal is determined by a very-high-frequency contribution $\epsilon'_\infty (=n^2$, where n is the refractive index) and a lattice, or infrared, contribution, ϵ'_1 , determined by the polar optical (TO) phonons. For most ionic crystals (e.g., alkali-metal and alkaline-earth-metal halides) ϵ'_∞ and ϵ' are roughly comparable, and usually below 10 in magnitude. However, there are known ionic solids, which are not ferroelectric, that have large ϵ 's. An example that is closest to being relevant for comparison to CCTO is rutile (TiO_2) in which the Ti^{4+} ion is surrounded by an oxygen octahedron as in CCTO. Rutile is a tetragonal crystal whose dielectric constants ϵ'_a and ϵ'_c , are large and decrease with increasing T . Specifically, ϵ'_a decreases from 114.9 to 110.6 and ϵ'_c decreases from 251 to 234 in going from 4 to 76 K.²² These ϵ 's are dominated by ϵ'_1 , which is determined by the existence of a relatively soft long-wavelength phonon mode in the TO phonon spectrum whose frequency decreases with decreasing T —a fact due to anharmonic lattice dynamical contributions.²² The general rule for *normal* ionic crystals is the opposite, i.e., a decreasing ϵ' with decreasing T due to stiffening of the phonon spectrum and a concomitant decrease in the lattice polarizability with decreasing volume (thermal contraction). Thus, we suggest that CCTO has some soft-mode character in its TO phonon spectrum. It is this soft-mode character that is responsible for the ~ 75 value of ϵ' and for its increase with decreasing T as shown in Fig. 8 in the T range above T_N —a situation akin to that in TiO_2 .

This indeed turns out to be the case. Homes *et al.*² studied the temperature dependence of the ir-active TO modes of CCTO. They find that whereas the higher-lying modes ($\omega \geq 300 \text{ cm}^{-1}$) harden and narrow with decreasing T , as expected for an ordinary ionic crystal, the low-lying modes, especially the lowest one with $\omega \approx 122 \text{ cm}^{-1}$, soften and broaden with decreasing T . This is characteristic of soft-mode behavior, albeit the degree of softening is small and is

consistent with the relatively small increase in ϵ' with decreasing T , as we observe.

Homes *et al.*² calculated the complex dielectric function from their ir data, modeling the modes as Lorentzian oscillators. They find that the low-frequency value of ϵ' at room temperature is ~ 75 , which increases to ~ 115 below 10 K. This low- T value is of the same order of magnitude, but somewhat higher than, the 75 we measure (see Fig. 8) on the 3 at. % Fe-doped sample. While Fe doping may contribute some to the difference, we do not believe that it accounts for its entirety. He *et al.*'s first-principles calculations⁶ yielded a lattice contribution of ~ 40 to ϵ' . Despite these numerical differences, we believe that our experimental results have finally established the intrinsic low-temperature dielectric response of CCTO, and it is ~ 75 .

The combination of the temperature and pressure dependence of ϵ' at low temperatures allows us to examine the above considerations further. The measured temperature dependence of ϵ' at constant pressure arises from two contributions,²² (i) the change that arises solely from the change in lattice spacing or density, i.e., the explicit volume effect, and (ii) the explicit temperature dependence that would occur even if the volume of the sample were to remain fixed. Writing $\epsilon' = \epsilon'(V, T)$ we then have

$$\left(\frac{\partial \ln \epsilon'}{\partial T} \right)_P = \left(\frac{\partial \ln V}{\partial T} \right)_P \left(\frac{\partial \ln \epsilon'}{\partial \ln V} \right)_T + \left(\frac{\partial \ln \epsilon'}{\partial T} \right)_V = -\frac{\beta}{\kappa} \left(\frac{\partial \ln \epsilon'}{\partial P} \right)_T + \left(\frac{\partial \ln \epsilon'}{\partial T} \right)_V \quad (1)$$

where $\beta \equiv (\partial \ln V / \partial T)_P$ is the volume thermal-expansion coefficient and $\kappa \equiv -(\partial \ln V / \partial P)_T$ is the isothermal volume compressibility. Thus, the constant-volume contribution $(\partial \ln \epsilon' / \partial T)_V$ can be evaluated from the measured isobaric and isothermal derivatives and a knowledge of β and κ .

It is physically meaningful to evaluate the two contributions in Eq. (1) for CCTO only in the intrinsic regime which is truly observed below ~ 80 K (Fig. 8). We should also stay away from the lowest T 's to avoid the AFM phase and because both β and $(\partial \epsilon' / \partial T) \rightarrow 0$ as $T \rightarrow 0$ K. Thus, the relevant intrinsic regime for our 3 at. % Fe sample exists over a narrow T range where we find that the second term, i.e., $(\partial \ln \epsilon' / \partial T)_V$, is by far the dominant term in determining $\epsilon'(T)$. We illustrate this at one temperature, 60 K. At this temperature, $\beta = 1 \times 10^{-6} / \text{K}$, $\kappa \approx 5 \times 10^{-4} / \text{kbar}$ (a typical value for a perovskite) and from our data, $(\partial \ln \epsilon' / \partial P) = -1 \times 10^{-2} / \text{kbar}$ and $(\partial \ln \epsilon' / \partial T)_P = -5 \times 10^{-4} / \text{K}$. Substituting these values in Eq. (1) yields $+0.2 \times 10^{-4} / \text{K}$ for the first term on the right-hand side and $-4.8 \times 10^{-4} / \text{K}$ for the second term $(\partial \ln \epsilon' / \partial T)_V$, clearly showing the dominance of this latter term. Noting that this term is proportional to $(\partial \ln \alpha / \partial T)_V$, where α is the polarizability, it is seen that unlike the case of ordinary ionic crystals, the polarizability of CCTO *decreases* with *increasing* T —a property of lattices that exhibit soft character in their long-wavelength TO phonon spectrum.²²

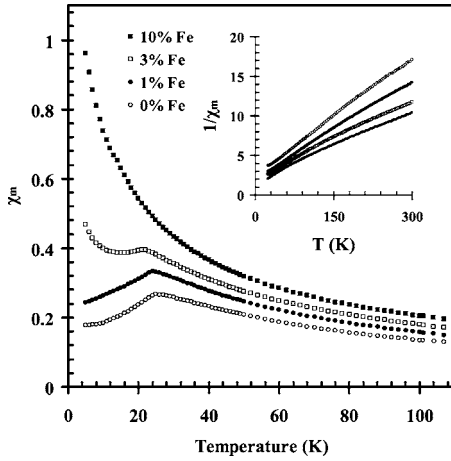


FIG. 12. Magnetic susceptibility versus temperature for undoped CCTO and samples with 1, 3, and 10 at. % Fe. Inset: inverse susceptibility for these four samples over an extended T range.

D. Magnetic properties (T_N and χ)

The magnetic molar susceptibility χ_m was measured from 5 to 300 K in an applied field of 10 mT to determine the effect of Fe doping on the magnetism in CCTO. Figure 12 compares the results for undoped CCTO and three doped samples containing 1%, 3%, and 10% Fe. In all cases, χ_m is plotted per mole of CCTO in dimensionless MKS units. The inset shows the inverse susceptibility versus temperature for the same four samples. The undoped sample shows classic AFM temperature dependence with a maximum near 25 K, in good agreement with earlier work.^{11–13} At low temperature χ_m for undoped CCTO falls to 2/3 of its maximum value, as expected for a polycrystalline AFM.

The Cu^{2+} ions in CCTO have an unusual triply degenerate T_{2g} ground state, leading to a strong coupling between the crystallographic and magnetic structures.²³ This strong coupling is observed in the low-temperature dielectric anomaly discussed above. In addition, the Cu superexchange interaction that leads to AFM ordering occurs mainly through the nonmagnetic Ti^{4+} ions.²⁵ Hence, substitution of Fe^{3+} on the Ti^{4+} B site should affect the AFM transition.

Figure 12 shows that the addition of Fe causes a monotonic increase in the susceptibility at all temperatures. Table II gives the Néel temperature T_N for the four samples. There is a marked decrease in T_N with increasing Fe content, consistent with Fe^{3+} occupying Ti^{4+} sites and thus disrupting the Cu superexchange interaction. The T_N values for undoped and 3% Fe-doped CCTO are in good agreement with the break in dielectric response at 24 and 21 K, respectively, as

discussed in Sec. III A. For undoped CCTO and samples with 1% and 3% Fe, T_N was determined from the local maximum in susceptibility. For the sample with 10% Fe, T_N was estimated from the slight break in $\chi_m(T)$ between 14 and 15 K (which is revealed more clearly in a χT vs T plot). This feature was present in repeated measurements on the same sample.

The susceptibility data for the undoped CCTO sample between 75 and 300 K were fitted to a Curie-Weiss equation plus a temperature-independent paramagnetism factor A ,

$$\chi_m(T) = A + C_{\text{Cu}}/(T + \theta_{\text{Cu}}) \quad (2)$$

where C_{Cu} is the Curie constant for the Cu ions and θ_{Cu} is the Curie-Weiss temperature. The least-squares fitting parameters were $A=0.015(3)$ per mole CCTO, $C_{\text{Cu}}=16.5(5)\text{K/mol CCTO}$, and $\theta_{\text{Cu}}=24(1)\text{K}$. Using a spin-only moment of 1.9 Bohr magnetons (μ_B) for spin-1/2 Cu^{2+} ions in an oxide host, the predicted Curie constant is 17.0 K/mol CCTO, in good agreement with our least-squares value and prior measurements on undoped CCTO.^{11–13} The origin of the temperature-independent paramagnetism, parameter A in Eq. (2), is not known.

Given the limited temperature range above T_N where Curie-Weiss fits are reasonable, the effect of Fe on χ_m was modeled by adding one additional parameter, a Curie term, C_{Fe}/T , to Eq. (2). This was motivated by the monotonic increase in $\chi_m(T)$ with decreasing T for the 10% Fe-doped CCTO sample (Fig. 12) and the expectation that Fe substituting on the Ti B site would not have significant exchange coupling to the Cu ions, i.e., any “Curie temperature” θ_{Fe} would be small. Table II shows the least-squares value C_{Fe} for the three Fe-doped CCTO samples, where the other parameters (A , C_{Cu} , and θ_{Cu}) were kept fixed at their values for undoped CCTO.

Fe^{3+} has an effective spin of $5.9 \mu_B$ in an oxide host and a calculated Curie constant of 211 K per mole of CCTO if all Ti^{4+} is replaced by Fe^{3+} , more than 12 times the value for Cu^{2+} . Hence, the 10% Fe-doped CCTO sample should have a value for C_{Fe} somewhat larger than the 16.5 measured for C_{Cu} . As shown in Table II, C_{Fe} is less than half the expected value. Fe^{2+} has a larger moment ($6.7 \mu_B$ versus $5.9 \mu_B$ for Fe^{3+} in oxide hosts), so the small value for C_{Fe} cannot be attributed to a portion of the Fe substituting as Fe^{2+} for A-site Cu^{2+} . This suggests that a substantial part of the Fe dopant is not incorporated into the CCTO host lattice.

E. Coupled dielectric-magnetic interactions

There is considerable recent interest in identifying materials that exhibit coupling between the polarization and

TABLE II. Néel temperature and Curie constant for undoped and Fe-doped CCTO samples.

Composition	T_N (K)	C_{Cu} (K/mol CCTO)	C_{Fe} (K/mol CCTO)
CCTO undoped	25.0(2)	16.5(5)	0
CCTO/1 % Fe	24.1(2)	16.5(5)	2.5(3)
CCTO/3 % Fe	21.9(2)	16.5(5)	4.3(3)
CCTO/10% Fe	14.6(5)	16.5(5)	7.0(3)

magnetization—the so-called magnetodielectric or multiferroic materials. Recent publications have identified the distorted perovskites $RMnO_3$ ($R=Y, Yb, \text{ and } Lu$) (Ref. 24) and $SeCuO_3$ and $TeCuO_3$ (Ref. 25) as compounds that exhibit such coupling. All of these compounds exhibit known AFM transitions (the exception being $SeCuO_3$ which exhibits a ferromagnetic transition) that are accompanied by small dielectric constant anomalies at their transition temperatures. The shape and character of the anomalies (decrease in ϵ' in the magnetically ordered phase over what it would be in the absence of magnetic order) are common to all of these materials and are similar to our own results on CCTO (Fig. 8). Another attempt to look for coupling between the polarization and magnetization is the recent fabrication of a composite structure made up of cobalt ferrite rods embedded in a $BaTiO_3$ matrix.²⁶ In this sample an anomaly is observed in ϵ' at the magnetic transition, but it is not clear that this is due to the sought-after coupling.

How do we understand this coupling in the distorted perovskites, including CCTO? In the case of the $RMnO_3$ compounds that have hexagonal crystal structures, it is found that there is an anomaly in $\epsilon'_{ab}(T)$ at $T \leq T_N$, but not in $\epsilon'_c(T)$, suggesting a unique correlation between the magnetization and polarization in the ab plane.²⁴ In contrast, our CCTO is an isotropic cubic material that should exhibit no anisotropy.

Katsufuji *et al.*²⁴ attribute the decrease in ϵ' of the $RMnO_3$ compounds below T_N to a decrease in the electronic dielectric constant ϵ'_∞ , with no contribution from the lattice (phonon) dielectric constant ϵ'_1 . The argument goes as follows. Given that $\epsilon'_\infty \propto 1/E_g^2$, where E_g is a charge excitation gap, an increase in E_g on AFM ordering (associated with charge transfer between the Mn 3d and 2p states) implies a decrease in ϵ'_∞ .

Lawes *et al.*²⁵ have interpreted the ϵ' anomalies at the FM transition in $SeCuO_3$ and the AFM transition in $TeCuO_3$ in terms of a phenomenological model based on a complex coupling between uniform polarization and wave-vector-dependent spin-spin correlation functions. Implied in their treatment is the notion that the influence of magnetic fluctuations sets in at $T > T_N$, with the thermal average of the spin-spin correlations, $\langle M_q M_{-q} \rangle$, developing q dependence that peaks near the magnetic Bragg vector at the zone boundary. It is suggested that the coupling leads to a decrease in ϵ' below T_N .

CCTO is a more complex oxide than the above-cited $RMnO_3$ and $TeCuO_3$ compounds but, due to a fortunate circumstance, this complexity leads to a more natural view of strong coupling between the crystallographic and magnetic structures. Specifically, as shown by Lacroix²³ in materials with orbital degeneracy, the crystallographic and magnetic structures are strongly connected, the exchange interactions being dependent on the occupied orbitals, which are related to the crystallographic distortions. In the case of triply degenerate T_{2g} states as in CCTO, the magnetic structure can be interpreted by taking into account the superexchange and the spin-orbit coupling.²³ The Ti^{4+} ions are in octahedral sites and their d orbitals are all empty (nonmagnetic), Cu^{2+} ions being the only magnetic ions in CCTO.

The superexchange interaction between Cu^{2+} ions occurs mainly through the Ti^{4+} ions, and this has consequences for

our present work. First, the substitution of Fe^{3+} for Ti^{4+} should affect T_N , and this is what we observe, as discussed in Sec. III D. Secondly, this coupling of the Cu^{2+} and Ti^{4+} ions should lead to some stiffening of the lattice (primarily the TiO_6 octahedra) on AFM ordering—an effect that will raise the soft-mode frequency, thereby reducing the lattice polarizability and lowering ϵ' in the AFM phase as observed in Fig. 8. We should also point out that the strong coupling between the magnetic and crystallographic structures can lead to changes in the lattice parameter(s) and structure of CCTO in the AFM phase, and such changes can also contribute to the observed $\epsilon'(T)$ anomaly below T_N . Clearly, diffraction studies of CCTO in the neighborhood of T_N would be of interest.

IV. CONCLUDING REMARKS

In this work we have investigated the influence of Fe and Nb doping and hydrostatic pressure on the dielectric response and magnetic properties of CCTO. Several features in the responses of this interesting material have been found. Here we provide a brief summary of the main findings and remaining issues.

(1). We have demonstrated that the unusual dielectric relaxation response of CCTO is indeed extrinsic and can be understood in terms of a simple capacitive-layer model consisting of conducting grains and insulating grain boundaries as also concluded by others.^{4,7,10}

(2). The energetics and kinetics of the main (low- T) relaxation process were determined. Two thermally activated regimes, related to different conduction processes in the CCTO grains, control the dynamics. It is suggested that these two regimes result from the emission of electrons from two energy levels associated with the oxygen vacancy in CCTO. A higher- T relaxation process was also discovered that is determined by grain boundary conduction.

(3). Both Nb and Fe doping lead to lower ϵ' in the plateau region and to lower dielectric losses, but increased Fe doping leads to the more dramatic effects. In particular, 3 at. % Fe makes CCTO an intrinsic very-low-loss dielectric and removes the anomalous $\epsilon'(\omega, T)$ response. It is suggested that the intrinsic behavior is due to carrier compensation in the grains, the Fe-produced holes compensating for the conduction electrons contributed by the oxygen vacancies.

(4). The intrinsic value of ϵ' (≈ 75 at low T) and its temperature dependence were determined. It is shown that this large ϵ' (compared to that of normal dielectrics where $\epsilon' \leq 10$) and its T dependence are largely determined by a low-lying, long-wavelength, soft TO phonon.

(5). A dielectric anomaly associated with the onset of antiferromagnetic order is observed below 24 K providing evidence of coupling between the polarization and sublattice magnetization. A plausible explanation for this anomaly is given.

(6). The Néel temperature of CCTO is essentially independent of Nb doping (up to 4 at. %) and of hydrostatic pressure (up to 7 kbar), but decreases significantly with increased Fe doping. At the highest Fe concentration (10

at. %), the results suggest decoupling of the Fe spins from the Cu spins, consistent with considerable Fe^{3+} substituting for Ti^{4+} .

Thus, we conclude that the present work has revealed many additional facets about the interesting properties of CCTO and has shed much light on the physics. More work is needed to more fully understand the electrical properties of both the grains and grain boundaries during ceramic processing. Studies on single crystals, when they become more readily available, could add additional insights.

Finally, we note that recently we became aware of a publication by Capsoni *et al.* on the role of doping in CCTO.²⁷ Two aspects of their results are relevant to our work and support our conclusions. Specifically, (1) using EPR they

find that Fe substitutes at the Ti site, and (2) Fe substitution in the 2–5 at. % range makes CCTO insulating with comparable bulk and grain boundary resistivities of more than $10^7 \Omega \text{ cm}$.

ACKNOWLEDGMENTS

This work was supported by the Sandia National Laboratories Directed R&D program and by the Division of Materials Sciences and Engineering, Office of Basic Energy Sciences, U.S. Department of Energy. Sandia National Laboratories is operated by Sandia Corporation, a Lockheed Martin Company, for the DOE's National Nuclear Security Administration under Contract No. DE-AC04-94AL85000.

-
- ¹M. A. Subramanian, D. Li, N. Duan, B. A. Reisner, and A. W. Sleight, *J. Solid State Chem.* **151**, 323 (2000).
 - ²C. C. Homes, T. Vogt, S. M. Shapiro, S. Wakimoto, and A. P. Ramirez, *Science* **293**, 673 (2001).
 - ³A. P. Ramirez, M. A. Subramanian, M. Gardel, G. Blumberg, D. Li, T. Vogt, and S. M. Shapiro, *Solid State Commun.* **115**, 217 (2000).
 - ⁴D. C. Sinclair, T. B. Adams, F. Morrison, and A. R. West, *Appl. Phys. Lett.* **80**, 2153 (2002).
 - ⁵S. Aygun, X. Tan, J. P. Maria, and D. P. Cann, in *Proceedings of the 204th Electrochemical Society Meeting* (Orlando, Florida, 2003).
 - ⁶L. He, J. B. Neaton, D. Vanderbilt, and M. H. Cohen, *Phys. Rev. B* **67**, 012103 (2003).
 - ⁷T. B. Adams, D. C. Sinclair, and A. R. West, *Adv. Mater. (Weinheim, Ger.)* **14**, 1321 (2002).
 - ⁸P. Lunkenheimer, V. Bobnar, A. V. Pronin, A. I. Ritus, A. A. Volkov, and A. Loidl, *Phys. Rev. B* **66**, 052105 (2002); see also P. Lunkenheimer, R. Fichtl, S. G. Ebbinghaus, and A. Loidl, *Phys. Rev. B* **70**, 172102 (2004).
 - ⁹M. H. Cohen, J. B. Neaton, L. He, and D. Vanderbilt, *J. Appl. Phys.* **94**, 3299 (2003).
 - ¹⁰S.-Y. Chung, I.-D. Kim, and S.-J. L. Kang, *Nat. Mater.* **3**, 774 (2004).
 - ¹¹A. Collomb, D. Samaras, B. Bochu, and J. C. Joubert, *Phys. Status Solidi A* **41**, 459 (1977).
 - ¹²Y. J. Kim, S. Wakimoto, S. M. Shapiro, P. M. Gehring, and A. P. Ramirez, *Solid State Commun.* **121**, 625 (2002).
 - ¹³M. C. Mozzati, C. B. Azzoni, D. Capsoni, M. Bini, and V. Massarotti, *J. Phys.: Condens. Matter* **15**, 7365 (2003).
 - ¹⁴G. H. Jonker, and E. E. Havinga, *Mater. Res. Bull.* **17**, 345 (1982).
 - ¹⁵N. H. Chan, R. K. Sharma, and D. M. Smyth, *J. Electrochem. Soc.* **128**, 1763 (1981).
 - ¹⁶D. Dimos, S. J. Lockwood, R. W. Schwartz, and M. S. Rogers, *IEEE Trans. Compon., Packag. Manuf. Technol., Part A* **18**, 174 (1995).
 - ¹⁷T. J. Boyle, P. G. Clem, B. A. Tuttle, G. L. Brennecke, J. T. Dawley, M. A. Rodriguez, T. D. Dumbbar, and W. F. Hammetter, *J. Mater. Res.* **17**, 871 (2002).
 - ¹⁸See, e.g., J. Volger, in *Progress in Semiconductors*, edited by A. F. Gibson (John Wiley and Sons, New York, 1960), Vol. 4, p. 207, and references therein.
 - ¹⁹A. J. Moulson and J. M. Herbert, *Electroceramics* (Chapman and Hall, New York, 1990), p. 41.
 - ²⁰S. A. Raevski, S. A. Prosandev, A. S. Bogatin, M. A. Malitskaya, and L. Jastrabik, *J. Appl. Phys.* **93**, 4130 (2003).
 - ²¹A. Tselev, C. M. Brooks, S. M. Anlage, H. Zheng, L. Salamanca-Riba, R. Ramesh, and M. A. Subramanian, *Phys. Rev. B* **70**, 144101 (2004).
 - ²²G. A. Samara and P. S. Peercy, in *Solid State Physics*, edited by H. Ehrenreich, R. Spaepen, and D. Turnbull (Academic Press, New York, 1981), Vol 36, p. 1. See also, *Phys. Rev. B* **7**, 1131 (1973).
 - ²³C. Lacroix, *J. Phys. C* **13**, 5125 (1980).
 - ²⁴T. Katsufuji, S. Mori, M. Masaki, Y. Moritomo, N. Yamamoto, and H. Takagi, *Phys. Rev. B* **64**, 104419 (2001).
 - ²⁵G. Lawes, A. P. Ramirez, C. M. Varma, and M. A. Subramanian, *Phys. Rev. Lett.* **91**, 257208 (2003).
 - ²⁶H. Xheng *et al.*, *Science* **303**, 661 (2004).
 - ²⁷D. Capsoni, M. Bini, V. Massarotti, G. Chiodelli, M. C. Mozzatic, and C. B. Azzoni, *J. Solid State Chem.* **177**, 4494 (2004).